

## MEDICAL IMAGE FUSION BASED ON RIPPLET TRANSFORM TYPE-I

S. Das\*, M. Chowdhury, and M. K. Kundu

Machine Intelligence Unit, Indian Statistical Institute, 203 B.T. Road, Kolkata-108, India

**Abstract**—The motivation behind fusing multimodality, multi-resolution images is to create a single image with improved interpretability. In this paper, we propose a novel multimodality Medical Image Fusion (MIF) method, based on Ripplet Transform Type-I (RT) for spatially registered, multi-sensor, multi-resolution medical images. RT is a new Multi-scale Geometric Analysis (MGA) tool, capable of resolving two dimensional ( $2D$ ) singularities and representing image edges more efficiently. The source medical images are first transformed by discrete RT (DRT). Different fusion rules are applied to the different subbands of the transformed images. Then inverse DRT (IDRT) is applied to the fused coefficients to get the fused image. The performance of the proposed scheme is evaluated by various quantitative measures like Mutual Information (MI), Spatial Frequency (SF), and Entropy (EN) etc. Visual and quantitative analysis shows, that the proposed technique performs better compared to fusion scheme based on Contourlet Transform (CNT).

### 1. INTRODUCTION

Different modalities of medical imaging reflect different information of human organs and tissues, and have their respective application ranges. For instance, structural images such as Magnetic Resonance Imaging (MRI), Computed Tomography (CT), Ultrasonography (USG), Magnetic Resonance Angiography (MRA) etc. provide high-resolution images with anatomical information. On the other hand, functional images such as Position Emission Tomography (PET), Single-Photon Emission Computed Tomography (SPECT) and

---

*Received 6 April 2011, Accepted 19 May 2011, Scheduled 22 May 2011*

\* Corresponding author: Sudeb Das (to.sudeb@gmail.com).

functional MRI (fMRI) etc. provide low-spatial resolution images with functional information [1]. A single modality of medical image cannot provide comprehensive and accurate information. As a result, combining anatomical and functional medical images to provide much more useful information through image fusion, has become the focus of imaging research and processing [2].

The main aim of Image fusion (IF) is integrating complementary, as well as redundant information from multiple images to create a fused image, providing more complete and accurate description. This fused image is more suitable for human visual and machine perception or further image processing and analysis tasks. Another advantage of image fusion is that it reduces the storage cost by storing only the single fused image, instead of the multisource images.

So far, many IF techniques have been proposed by various researchers in the literature. Generally, IF methods can be classified into three categories based on the merging state: pixel or sensor level, feature level, and decision level [3]. It has been found, that the pixel-level spatial domain IF methods usually leads to contrast reduction [4]. Methods based on Intensity-Hue-Saturation (IHS), Principal Component Analysis (PCA), and the Brovey Transform offers better results, but, suffers from spectral degradation [5]. Many Multiresolution Analysis (MRA) based IF methods have been proposed to improve the fusion result. Pyramidal IF schemes such that the laplacian pyramid, the gradient pyramid, the contrast pyramid, etc. fails to introduce any spatial orientation selectivity in the decomposition process, and hence often causes blocking effects [6]. The other MRA-tool, that has been used in IF extensively is the Discrete Wavelet Transform (DWT) [7, 8]. The problem with Wavelet Transform (WT) is that, it can preserve spectral information efficiently but cannot express spatial characteristics well. The isotropic WT is scant of shift-invariance and multidirectionality, and fail to provide an optimal expression of highly anisotropic edges and contours in images. So, WT based fusion scheme cannot preserve the salient features of the source images efficiently, and will probably introduce some artifacts and inconsistency in the fused results [9, 15].

Recently, a theory called Multi-scale Geometric Analysis (MGA) for high-dimensional signals has been developed, and several MGA tools were proposed like Ridgelet, Curvelet, Bandlet, Brushlet and Contourlet. These MGA tools does not suffer from the problems of WT. Few MIF methods based on these MGA tools were also proposed to improve the fusion result [9, 10].

In this paper, we propose a novel MIF method based on a recently developed MGA tool called Ripplet Transform Type-I (RT).

RT is proposed by Jun Xu et al. to address the problem faced by the conventional transforms, like Fourier transform (FT) and WT, regarding the discontinuities such as edges and contours in the images [11]. To our knowledge, this is the first attempt to apply RT to fuse multimodality medical images. The source medical images are first transformed by DRT. Every possible combination of four different (simple average, maximum selection, PCA and addition) primitive fusion rules, are applied to the Low-frequency (LF)-subband and High-frequency (HF)-subbands coefficients of the transformed images, to get the fused coefficients. The final fused images are obtained by applying Inverse DRT (IDRT) on the fused coefficients. A comparison of the effectiveness of the fusion rules, used in the paper is carried out. Both visual and quantitative performance evaluations are made and verified in the paper. Performance comparison of the proposed RT based method with CNT based fusion schemes, shows that the proposed method performs better.

The rest of the paper is organized as follows. RT is described in Section 2. Section 3 presents the proposed algorithm. Experimental results and comparisons are given in Section 4 and we draw conclusion in Section 5.

## 2. RIPPLET TRANSFORM TYPE-I (RT)

Conventional transforms like FT and WT suffer from discontinuities such as edges and contours in images. To address this problem, Jun Xu et al. proposed a new MGA-tool called RT. The RT is a higher dimensional generalization of the Curvelet Transform (CVT), capable of representing images or  $2D$  signals at different scales and different directions. To achieve anisotropic directionality, CVT uses a parabolic scaling law. From the perspective of microlocal analysis, the anisotropic property of CVT guarantees resolving  $2D$  singularities along  $C^2$  curves [12]. On the other hand, RT provides a new tight frame with sparse representation for images with discontinuities along  $C^d$  curves [11].

There are two questions regarding the scaling law used in CVT: 1) Is the parabolic scaling law optimal for all types of boundaries? and if not, 2) What scaling law will be optimal? To address these questions, Jun Xu et al. intended to generalize the scaling law, which resulted in RT. RT generalizes CVT by adding two parameters, i.e., support  $c$  and degree  $d$ . CVT is just a special case of RT with  $c = 1$  and  $d = 2$ . The anisotropy capability of representing singularities along arbitrarily shaped curves of RT is due to these new parameters  $c$  and  $d$ .

### 2.1. Continuous Ripplet Transform (CRT)

For a 2D integrable function  $f(\vec{x})$ , the CRT is defined as the inner product of  $f(\vec{x})$  and ripples  $\rho_{a\vec{b}\theta}(\vec{x})$  as given below [11]

$$R(a, \vec{b}, \theta) = \langle f, \rho_{a\vec{b}\theta} \rangle = \int f(\vec{x}) \overline{\rho_{a\vec{b}\theta}(\vec{x})} d\vec{x}, \tag{1}$$

where  $R(a, \vec{b}, \theta)$  are the ripplet coefficients and  $\overline{(\cdot)}$  denotes the conjugate operator. The ripplet function of the Equation (1) is defined as

$$\rho_{a\vec{b}\theta}(\vec{x}) = \rho_{a\vec{0}0}(R_\theta(\vec{x} - \vec{b})), \tag{2}$$

where  $\rho_{a\vec{0}0}(\vec{x})$  is the ripplet element function,  $R_\theta = \begin{bmatrix} \cos \theta & \sin \theta \\ -\sin \theta & \cos \theta \end{bmatrix}$  is the rotation matrix,  $\vec{x}$  and  $\vec{b}$  are 2D vectors;  $b$  and  $\theta$  denotes the position parameter and rotation parameter respectively. The element ripplet function is defined in frequency domain as

$$\hat{\rho}_a(r, \omega) = \frac{1}{\sqrt{c}} a^{\frac{1+d}{2d}} W(a \cdot r) V\left(\frac{a^{\frac{1}{d}}}{c \cdot a} \cdot \omega\right), \tag{3}$$

where  $\hat{\rho}_a(r, \omega)$  are the FT of  $\rho_{a\vec{0}0}(\vec{x})$  in polar coordinate system, and  $a$  is the scale parameter.  $W(r)$  is the ‘radial-window’ and  $V(\omega)$  is the ‘angular window’. These two windows have compact supports on  $[\frac{1}{2}, 2]$  and  $[-1, 1]$  respectively. They satisfy the following admissibility conditions:

$$\int_{\frac{1}{2}}^2 W^2(r) \frac{dr}{r} = 1, \tag{4}$$

$$\int_{-1}^1 V^2(t) dt = 1, \tag{5}$$

These two windows partition the polar frequency domain into ‘wedges’ as shown in Figure 1(a).

The ripples functions decay very fast outside the elliptical effective region, which has the following property for its length and width:  $width \approx length^d$ . Length and width is the major and minor axis of the ellipse respectively. The customizable effective region tuned by support  $c$  and degree  $d$  bespeaks the most distinctive property of ripples the general scaling. For  $c = 1, d = 1$ , both axis directions are scaled in the same way. So ripplet with  $d = 1$  will not have the anisotropic behavior. For  $d > 1$ , the anisotropic property is reserved for RT. For  $d = 2$ , ripples have parabolic scaling; for  $d = 3$ , ripples have cubic scaling; and so forth.

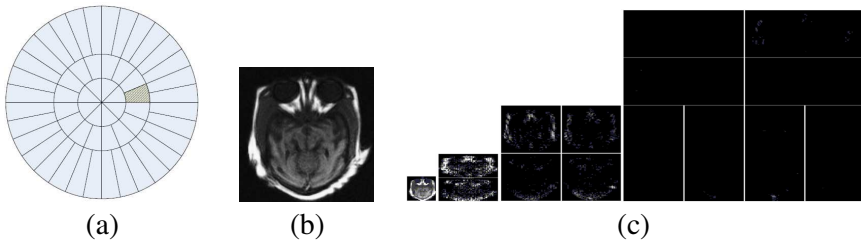


**Figure 1.** (a) The tiling of polar frequency domain. The shadowed ‘wedge’ corresponds to the frequency transform of the element function. Ripplet transform: (b) MRI image. (c) Different subbands after decomposition.

The CRT can only capture the characteristics of high frequency components of  $f(\vec{x})$ , since the scale parameter  $a$  cannot take the value of infinity. So the ‘full’ CRT consists of fine scale RT and coarse scale isotropic WT. We can perfectly reconstruct the input function based on its ripplet coefficients. If  $f(\vec{x}) \in L^2$  is a high-pass function i.e., its FT vanishes for  $|\omega| < \frac{2}{a_0}$  and  $a_0$  is a constant, then  $f(\vec{x})$  can be reproduced by its RT through

$$f(\vec{x}) = \int R(a, \vec{b}, \theta) \rho_{a \vec{b} \theta}(\vec{x}) da d\vec{b} d\theta / a^3, \tag{6}$$

and a Parseval formula for  $f$  holds

$$\|f\|_{L_2}^2 = \int |R(a, \vec{b}, \theta)|^2 da d\vec{b} d\theta / a^3, \tag{7}$$

### 2.2. Discrete Ripplet Transform (DRT)

As digital image processing needs discrete transform instead of continuous transform, here we describe the discretization of RT [11].

The discretization of CRT is based on the discretization of the parameters of ripplet functions.  $a$  is sampled at dyadic intervals.  $b$  and  $\theta$  are sampled at equal-spaced intervals.  $a_j, \vec{b}_k$  and  $\theta_l$  substitute  $a, \vec{b}$  and  $\theta$  respectively, and satisfy that  $a_j = 2^{-j}, \vec{b}_k = [c \cdot 2^{-j} \cdot k_1, 2^{-j/d} \cdot k_2]^T$  and  $\theta_l = \frac{2\pi}{c} \cdot 2^{-\lfloor j(1-1/d) \rfloor} \cdot l$ , where  $\vec{k} = [k_1, k_2]^T$ , and  $j, k_1, k_2, l \in \mathbb{Z}$ .  $(\cdot)^T$  denotes the transpose of a vector.  $d \in \mathbb{R}$ , since any real number can be approximated by rational numbers, so we can represent  $d$  with  $d = n/m, n, m \neq 0 \in \mathbb{Z}$ . Usually, we prefer  $n, m \in \mathbb{N}$  and  $n, m$  are both primes. In the frequency domain, the corresponding

frequency response of ripple function is in the form

$$\widehat{\rho}_j(r, \omega) = \frac{1}{\sqrt{c}} a^{\frac{m+n}{2n}} W(2^{-j} \cdot r) V\left(\frac{1}{c} \cdot 2^{-\lfloor j \frac{m-n}{n} \rfloor} \cdot \omega - l\right), \quad (8)$$

where  $W$  and  $V$  satisfy the following admissibility conditions:

$$\sum_{j=0}^{+\infty} |W(2^{-j} \cdot r)|^2 = 1, \quad (9)$$

$$\sum_{l=-\infty}^{+\infty} \left| V\left(\frac{1}{c} \cdot 2^{-\lfloor j(1-1/d) \rfloor} \cdot \omega - l\right) \right|^2 = 1, \quad (10)$$

given  $c$ ,  $d$  and  $j$ .

The ‘wedge’ corresponding to the ripple function in the frequency domain is

$$H_{j,l}(r, \theta) = \left\{ 2^j \leq |r| \leq 2^{2j}, \left| \theta - \frac{\pi}{c} \cdot 2^{-\lfloor j(1-1/d) \rfloor} \cdot l \right| \leq \frac{\pi}{2} 2^{-j} \right\}, \quad (11)$$

The DRT of an  $M \times M$  image  $f(n_1, n_2)$  will be in the form of

$$R_{j, \vec{k}, l} = \sum_{n_1=0}^{M-1} \sum_{n_2=0}^{N-1} f(n_1, n_2) \overline{\rho_{j, \vec{k}, l}(n_1, n_2)}, \quad (12)$$

where  $R_{j, \vec{k}, l}$  are the ripple coefficients.

The image can be reconstructed through Inverse Discrete Ripple Transform (IDRT)

$$\tilde{f}(n_1, n_2) = \sum_j \sum_{\vec{k}} \sum_l R_{j, \vec{k}, l} \rho_{j, \vec{k}, l}(n_1, n_2), \quad (13)$$

The Figures 1(b) and 1(c) show an MRI image and subbands of the ripple transformed MRI image after decomposition, respectively.

### 3. PROPOSED METHOD

The notations used in this section are as follows:  $A, B, F$  represents the two source images and the fused image respectively.  $C_X^Y(p)$  denotes the subbands of the images after applying DRT. ( $X = A, B, F$ ) and ( $Y = L, H$ ) where  $L$  and  $H$  represents the LF-subband and HF-subbands respectively.  $p = (m, n, k, l)$ , where  $(m, n)$  denotes the spatial location of each coefficients, and  $k$  the directional subbands at scale  $l$ . The method can be easily extended to more than two images.

In this section we first describe the fusion rules used in our method, and then we outline the steps of the proposed algorithm.

### 3.1. Fusion Rules

We have used four different primitive fusion rules in our proposed method. The reason behind choosing these simple fusion rules is that, as this is the first time RT is used to fuse images, so using these simple fusion rules we can understand how effective RT is in image fusion domain. The different fusion rules used in the proposed method are as follows:

#### 3.1.1. Simple Average (R1)

Simple average fusion rule gives equal importance to both the source images, and can be expressed as follows:

$$C_F^Y(p) = \frac{1}{2}(C_A^Y(p) + C_B^Y(p)), \tag{14}$$

#### 3.1.2. Maximum Selection Rule (R2)

According to this fusion rule, select the frequency coefficients from  $C_A^Y(p)$  and  $C_B^Y(p)$  with greater absolute value as the fused coefficients:

$$C_F^Y(p) = \left\{ \begin{array}{ll} C_A^Y(p) & |C_A^Y(p)| \geq |C_B^Y(p)| \\ C_B^Y(p) & |C_B^Y(p)| > |C_A^Y(p)| \end{array} \right\}, \tag{15}$$

#### 3.1.3. PCA Based Fusion Rule (R3)

PCA is a vector space transform often used to reduce multidimensional data sets to lower dimension for analysis. It reveals the internal structure of data in an unbiased way [13]. Assuming  $i$  and  $j$  as the the elements of the principal eigenvector, which are computed by analyzing the corresponding subbands  $C_A^Y(p)$  and  $C_B^Y(p)$  for corresponding coefficients, we obtain,

$$\alpha = \frac{i}{i+j} \quad \text{and} \quad \beta = \frac{j}{i+j} \tag{16}$$

$\alpha$  and  $\beta$  are the normalized weights used for fusing the source subbands, to get the fused coefficients:

$$C_F^Y(p) = \alpha \cdot C_A^Y(p) + \beta \cdot C_B^Y(p), \tag{17}$$

#### 3.1.4. Addition Rule (R4)

In this fusion rule, the fused coefficients are obtained by simply adding the corresponding source subbands coefficients:

$$C_F^Y(p) = C_A^Y(p) + C_B^Y(p), \tag{18}$$

To facilitate the description of the proposed algorithm, the above mentioned fusion rules are denoted by  $R_i$  where  $i = 1, 2, 3, 4$ ; as indicated in the headings of the fusion rules. The combinations of fusion rules are indicated by  $R_iR_j$  where  $i, j = 1, 2, 3, 4$ .

### 3.2. Proposed Fusion Algorithm

The medical images to be fused must be registered to assure that the corresponding pixels are aligned. Here we outline the salient steps of the proposed MIF method:

- (i) The registered source medical images  $A$  and  $B$  are decomposed by DRT to get the LF-subband and HF-subbands.
- (ii) The LF-subband and HF-subbands are fused using the different combinations of fusion rules (e.g.,  $R_1R_1$  to  $R_4R_4$ ).
- (iii) IDRT is applied to get the final fused medical image.

The block diagram of the proposed MIF scheme is shown in Figure 2.

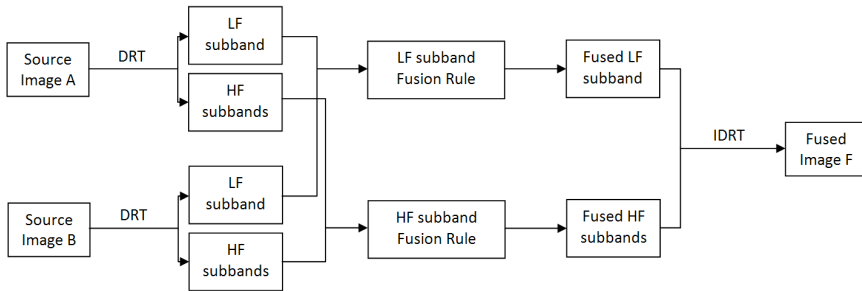


**Figure 2.** Block diagram of the proposed MIF method using RT.

## 4. EXPERIMENTAL RESULTS AND COMPARISONS

To evaluate the performance of the proposed MIF method, extensive experiments were carried out on various modalities of medical images. Figures 3((a), (b)) and 3((c), (d)) show two different sets of source images used in the experiments, and are denoted by  $IS_1$  and  $IS_2$ , respectively. The CT image in Figure 3(a) shows the bones and the MRI image in Figure 3(b) displays the soft tissues information. The T1-weighted MR image in Figure 3(c) of  $IS_2$  contains the soft tissues but no illness information, and the MRA image in Figure 3(d) shows the illness information (shown by the marked ellipse) but no soft tissues information. The decomposition parameter of DRT was  $levels = [1, 2, 4, 4]$ . The proposed scheme is compared with MIF



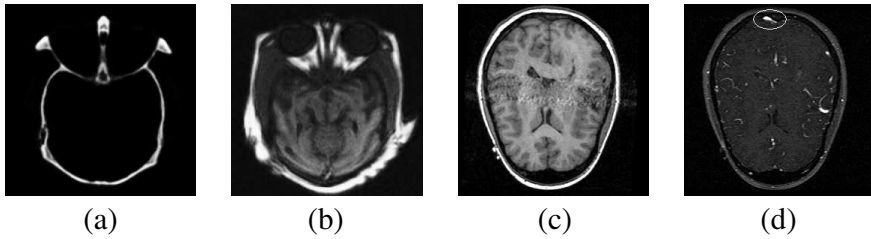


**Figure 3.** Source images: (a) CT image; (b) MRI image; (c) T1-weighted MR image; (d) MRA image. ((a), (b)) first set  $IS1$  and ((c), (d)) second set  $IS2$  of images, respectively (downloaded from <http://www.imagefusion.org/>).

method based on CNT. To show the effectiveness of the proposed technique, visual as well as quantitative analysis were carried out. The selected quantitative criterions used in the experiments are as follows:

#### 4.1. Standard Deviation (STD)

It measures the contrast in the fused image. An image with high contrast would have a high standard deviation.

$$STD = \sqrt{\frac{1}{MN} \sum_{m=1}^M \sum_{n=1}^N (F(m, n) - MEAN)^2}, \quad (19)$$

where  $M \times N$  denotes the size of the image and  $F(m, n)$  indicates the gray-value of the pixel of image  $F$  at position  $(m, n)$  and

$$MEAN = \frac{1}{MN} \sum_{m=1}^M \sum_{n=1}^N |F(m, n)|, \quad (20)$$

#### 4.2. Entropy (EN)

The entropy of an image is a measure of information content. It is the average number of bits needed to quantize the intensities in the image. It is defined as

$$EN = - \sum_{g=0}^{L-1} p(g) \log_2 p(g), \quad (21)$$

where  $p(g)$  is the probability of grey-level  $g$ , and the range of  $g$  is  $[0, \dots, L - 1]$ . An image with high information content would have high entropy. If entropy of fused image is higher than parent images then it indicates that the fused image contains more information.

### 4.3. Spatial Frequency (SF)

Spatial frequency can be used to measure the overall activity and clarity level of an image. Larger SF value denotes better fusion result:

$$SF = \sqrt{RF^2 + CF^2}, \quad (22)$$

where RF is the row frequency and CF is the column frequency:

$$RF = \sqrt{\frac{1}{M(N-1)} \sum_{m=0}^{M-1} \sum_{n=0}^{N-2} (F(m, n+1) - F(m, n))^2}, \quad (23)$$

and

$$CF = \sqrt{\frac{1}{(M-1)N} \sum_{m=0}^{M-2} \sum_{n=0}^{N-1} (F(m+1, n) - F(m, n))^2}, \quad (24)$$

where  $M \times N$  denotes the size of the image and  $F(m, n)$  indicates the gray-value of the pixel of image  $F$  at position  $(m, n)$ .

### 4.4. Mutual Information (MI)

It measures the degree of dependence of the two images. A larger measure implies better quality. Given two images  $x_F$  and  $x_R$  MI is defined as [14]:

$$MI = I(x_A; x_F) + I(x_B; x_F), \quad (25)$$

where

$$I(x_R; x_F) = \sum_{u=1}^L \sum_{v=1}^L h_{R,F}(u, v) \log_2 \frac{h_{R,F}(u, v)}{h_R(u)h_F(v)}, \quad (26)$$

where  $h_R$ ,  $h_F$  are the normalized gray level histograms of  $x_R$  and  $x_F$ , respectively.  $h_{R,F}$  is the joint gray level histogram of  $x_R$  and  $x_F$ , and  $L$  is the number of bins.  $x_R$  and  $x_F$  correspond to the reference and fused images, respectively.  $I(x_R; x_F)$  indicates how much information the fused image  $x_F$  conveys about the reference  $x_R$ . Thus, the higher the mutual information between  $x_F$  and  $x_R$ , the more likely  $x_F$  resembles the ideal  $x_R$ .

Quantitative and visual analysis of performance of the proposed scheme shows that, the combinations  $RiR3$ ,  $i = 1, 2, 3, 4$ ; of fusion rules, which use 'PCA Based Fusion Rule' ( $R3$ ) for HF-subband coefficients, gives the worst fused results, although in some cases provides high quantitative measure values. Figure 4 shows the fused images obtained by using  $RiR3$ ,  $i = 1, 2, 3, 4$ ; combinations of fusion rules. The fused images shown in Figures 4((a1)–(d1)) of  $IS1$  are very

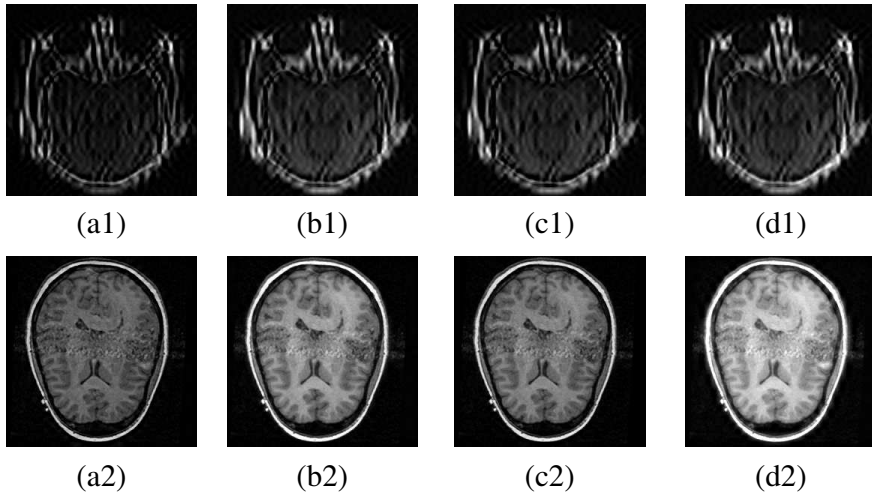


**Figure 4.** Results of using ‘PCA based fusion rule’ for HF-subbands coefficients: ((a1), (a2))  $R1R3$ ; ((b1), (b2))  $R2R3$ ; ((c1), (c2))  $R3R3$ ; ((d1), (d2))  $R4R3$ . ((a1)–(d1)) Fused images of  $IS1$  and ((a2)–(d2)) fused images of  $IS2$ .

distorted. For images of  $IS2$  the fused results shown in Figures 4((a2)–(d2)) are not so much distorted, but the illness information has been totally lost. Similar results have been obtained for other source images used in the experiments. From the fused results given above we may say that ‘PCA Based Fusion Rule’ for HF-subband coefficients is not suitable for MIF. So, in rest of the analysis of the experimental results we have excluded the results obtained by using the combination of fusion rules  $RiR3$ ,  $i = 1, 2, 3, 4$ .

The graphs of the Figure 5, Figure 6, Figure 7, and Figure 8 show the detailed quantitative analysis of the performance of the combinations of fusion rules  $RiRj$ ,  $i = 1, 2, 3, 4$ ; and  $j = 1, 2, 4$ ; for the first set of images  $IS1$ . Performance of both the MIF methods based on RT and CNT is presented in the graphs. It is clear from the graphs, that the combination  $R4Rj$ ,  $j = 1, 2, 4$ ; of fusion rules, which use ‘Addition Rule’  $R4$  for the LF-subband coefficients gives the better results among all the different combinations. It is also clear from the graphs that the MIF method based on RT, gives better result than the CNT based method. Only in some cases the quantitative measures obtained from CNT based MIF method perform better than the RT based proposed MIF scheme. Similar results have been obtained for  $IS2$  and other source images used in the experiments, where RT performs comparably with CNT.

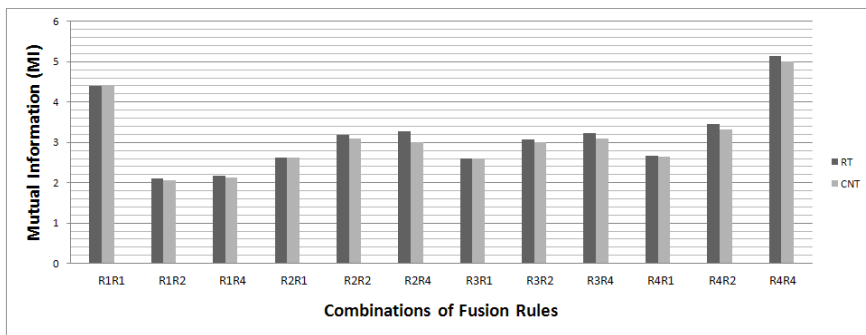


**Figure 5.** Performance analysis in respect to mutual information (MI).

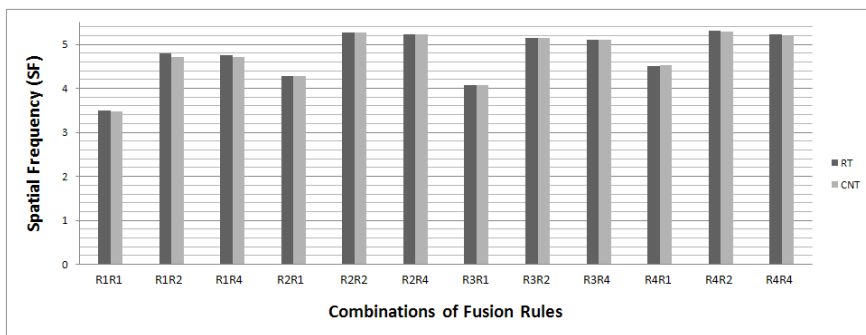


**Figure 6.** Performance analysis in respect to spatial frequency (SF).

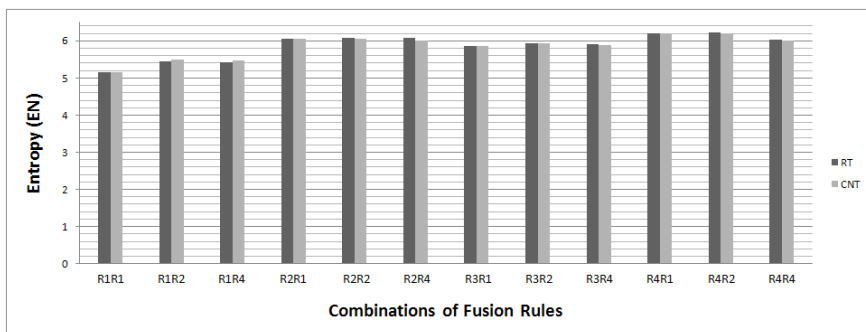


**Figure 7.** Performance analysis in respect to entropy (EN).

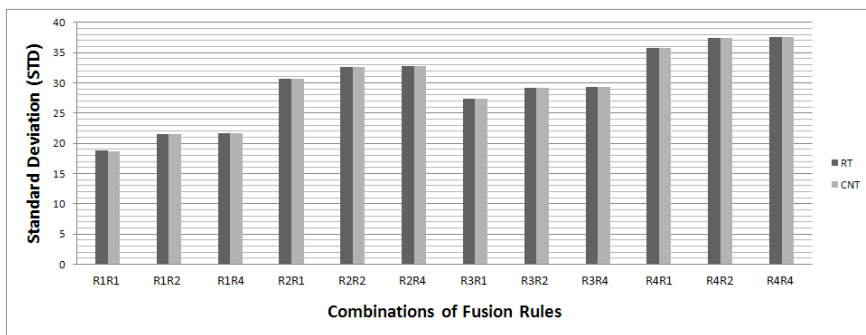


**Figure 8.** Performance analysis in respect to standard deviation (STD).

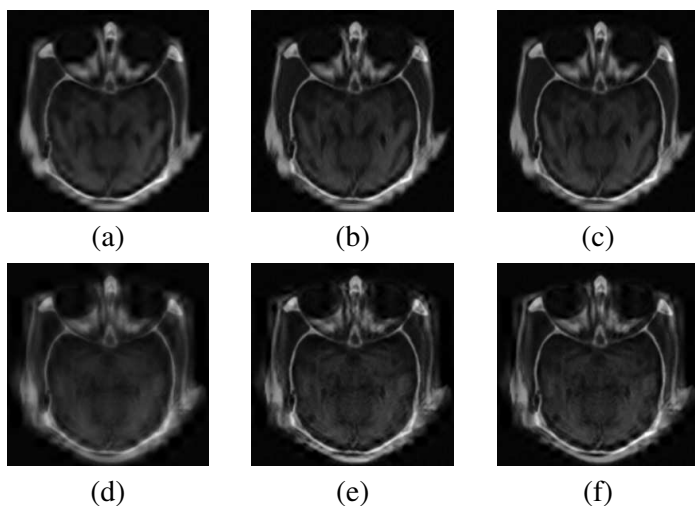


**Figure 9.** Results of using ‘addition rule’ for LF-subband coefficients: ((a)–(c)) for RT based MIF method and ((d)–(f)) for CNT based MIF method, ((a), (d))  $R4R1$ ; ((b), (e))  $R4R2$ ; ((c), (f))  $R4R4$ .

Figure 9 shows the fused images of *IS1*, obtained by applying the combinations of fusion rules  $R4Rj$ ,  $j = 1, 2, 4$ ; for both MIF methods based on RT and CNT, respectively. It can be easily seen that the fused images obtained using the proposed MIF method based on RT, is better than the CNT based scheme. We can see that the salient features and detailed information presented in Figures 9((a)–(c)) is much richer than Figures 9((d)–(f)). For the other sets of source images used in the experiments, similar results have been found.

**Table 1.** Performance comparison of RT and CNT based MIF method using the combinations  $R4Rj$ ,  $j = 1, 2, 4$ ; for  $IS1$  and  $IS2$ .

Image Set $IS1$						
		Fused By $R4R1$	Fused By $R4R2$	Fused By $R4R4$	Original Image 1	Original Image 2
SF	RT	4.5132	<b>5.3044</b>	<b>5.2343</b>	3.5472	4.3389
	CNT	<b>4.5319</b>	5.2999	5.2140		
EN	RT	<b>6.2071</b>	<b>6.2189</b>	<b>6.0215</b>	1.7126	5.6561
	CNT	6.1838	6.1817	6.0197		
STD	RT	<b>35.7651</b>	<b>37.4298</b>	37.5125	20.4484	30.3225
	CNT	35.7649	37.4001	<b>37.6070</b>		
Image Set $IS2$						
SF	RT	7.1979	<b>8.5422</b>	<b>8.7554</b>	7.7005	6.4901
	CNT	<b>7.2016</b>	8.5246	8.6979		
EN	RT	<b>6.9863</b>	<b>6.9642</b>	6.5065	4.1524	4.3310
	CNT	6.9704	6.9146	<b>6.6295</b>		
STD	RT	83.3503	84.5689	<b>85.7223</b>	69.1972	25.5812
	CNT	<b>83.3564</b>	<b>84.5808</b>	84.7133		

Table 1 shows the effectiveness of the proposed MIF method based on RT considering only the combinations  $R4Rj$ ,  $j = 1, 2, 4$ ; of fusion rules for both the image sets  $IS1$  and  $IS2$ , respectively. Performance analysis of both the MIF methods based on RT and CNT are compared in the Table 1. The ‘bold’ values indicate the higher values in the Table 1. The higher values of SF indicates that the fused images have more activity and clarity level than the source images. Similarly the higher values of EN and STD for the fused images show that the fused images have more information, as well as higher contrast than the source images. So, it is clear from Table 1 that, the fused images obtained by MIF methods based on RT as well as CNT are more clear, informative and have higher contrast which is helpful in visualization and interpretation. It is also obvious from the Table 1 that the proposed MIF methods based on RT perform comparably, and often better than CNT based MIF methods. For subjective analysis, the source images and the fused images obtained by our proposed MIF method as well as by CNT based MIF method were shown to an expert. After careful manual inspection, the expert conformed to the effectiveness of the proposed MIF method based on RT.

## 5. CONCLUSION

The fusion of multimodality medical images plays an critical and vital role in many clinical applications for they can support more comprehensive and accurate information than any individual source images. As a novel MGA-tool, ripplelet offers better advantage of directionality, localization, multiscale and anisotropy, which cannot be perfectly achieved by traditional MRA-tool like wavelet transform. In this paper, we propose a novel multimodality MIF method based on ripplelet transform type-I. Combinations of four different fusion rules are applied to fuse the different subbands. Even though, we have only used simple fusion rules in this paper, the experimental results show that RT is very effective in MIF. The proposed MIF method based on RT, is analyzed both visually and quantitatively. The proposed method is compared with CNT, and the superiority of the proposed method is established. Experimental results show that the RT based MIF, can preserve more useful information in the fused medical image with higher spatial resolution and less difference to the source images.

## ACKNOWLEDGMENT

We would like to thank Jun Xu and Depeng Wu (Dept. of Electrical and Computer Engineering, University of Florida, USA) for helping us in the implementation of Ripplelet Transform.

## REFERENCES

1. Daneshvar, S. and H. Ghassemian, "MRI and PET image fusion by combining IHS and retina-inspired models," *Information Fusion*, Vol. 11, No. 2, 114–123, April 2010.
2. Barra, V. and J. Y. Boire, "A general framework for the fusion of anatomical and functional medical images," *NeuroImage*, Vol. 13, No. 3, 410–424, March 2001.
3. Shivappa, S. T., B. D. Rao, and M. M. Trivedi, "An iterative decoding algorithm for fusion of multimodal information," *EURASIP Journal on Advances in Signal Processing*, Vol. 2008, Article ID 478396, 10 pages, 2008.
4. Li, S. and B. Yang, "Multifocus image fusion using region segmentation and spatial frequency," *Proceedings of Image Vision Computing*, Vol. 26, No. 7, 971–979, July 2008.
5. Yonghong, J., "Fusion of landsat TM and SAR image based on

- principal component analysis,” *Remote Sensing Technology and Application*, Vol. 13, No. 1, 46–49, March 1998.
6. Li, H., B. S. Manjunath, and S. K. Mitra, “Multisensor image fusion using the wavelet transform,” *Proceedings of CVGIP: Graphical Model and Image Processing*, Vol. 57, No. 3, 235–245, May 1995.
  7. Yang, Y., D. S. Park, S. Huang, and N. Rao, “Medical image fusion via an effective wavelet-based approach,” *EURASIP Journal on Advances in Signal Processing*, Vol. 2010, Article ID 579341, 13 pages, 2010.
  8. Amolins, K., Y. Zhang, and P. Dare, “Wavelet based image fusion techniques — An introduction, review and comparison,” *ISPRS Journal of Photogrammetry and Remote Sensing*, Vol. 62, No. 4, 249–263, September 2007.
  9. Yanga, L., B. L. Guoa, and W. Ni, “Multimodality medical image fusion based on multiscale geometric analysis of contourlet transform,” *Neurocomputing*, Vol. 72, Nos. 1–3, 203–211, December 2008.
  10. Ali, F. E., I. M. El-Dokany, A. A. Saad, and F. E. Abd El-Samie, “Curvelet fusion of MR and CT images,” *Progress In Electromagnetics Research C*, Vol. 3, 215–224, 2008.
  11. Xu, J., L. Yang, and D. Wu, “Ripplet: A new transform for image processing,” *Journal of Visual Communication and Image Representation*, Vol. 21, No. 7, 627–639, October 2010.
  12. Starck, J. L., E. J. Candes, and D. L. Donoho, “The curvelet transform for image denoising,” *IEEE Transactions on Image Processing*, Vol. 11, No. 6, 670–684, June 2002.
  13. Shlens, J., “A tutorial on principal component analysis,” <http://www.sn1.salk.edu/~shlens/pca.pdf>
  14. Qu, G. H., D. L. Zhang, and P. F. Yan, “Information measure for performance of image fusion,” *Electronic Letters*, Vol. 38, No. 7, 313–315, 2002.
  15. Kumar, G. R. H. and D. Singh, “Quality assessment of fused image of modis and palsar,” *Progress In Electromagnetics Research B*, Vol. 24, 191–221, 2010.